Research Article

Nanosize La-filled $CoSb_3$ skutterudite fabricated by electrospinning

Ana C. Ferreira[1,2] · Joaquim B. Branco[1,2] · António P. Gonçalves[1]

Received: 26 April 2020 / Accepted: 12 August 2020 / Published online: 1 September 2020

Abstract
Nanostructured binary skutterudites represented by MX_3 are potential thermoelectric materials for high efficiency thermoelectric. In this work, we synthesized for the first-time high purity nanofibers of $CoSb_3$ and rare earth filled $LaCo_4Sb_{12}$ with external diameters < 100 nm via electrospinning which provides a simple, easy to implement and versatile technique to develop novel nanostructured-based thermoelectric materials.

Keywords Thermoelectric materials · Skutterudite · Electrospinning · Nanofibers

1 Introduction

Binary skutterudite type compounds, represented by MX_3 (M = Co, Rh or Ir and X = P, As or Sb), are bulk semiconductors with cage-type crystal structures that possess high carrier mobilities, which is important for the development of new, high efficiency, thermoelectric devices [1]. Possible applications of such devices include the harvesting of the waste heat generated in industrial processes, automotive operations, and alternative refrigeration that could avoid the use of environmentally hazardous gases [2–5]. Among skutterudite structure compounds [6], $CoSb_3$ has attracted considerable attention in recent years due to its high Seebeck coefficient and electrical conductivity [1, 3, 7]. However, for practical applications, its high thermal conductivity (10–25 Wm^{-1} K^{-1} at room temperature) [8, 9] needs to be reduced to further increase the efficiency. In fact, the performance of thermoelectric materials can be defined by the figure of merit $zT = S^2\sigma T/\kappa$, where S is the Seebeck coefficient, σ and κ are the electrical and thermal conductivities, T is the absolute temperature. Considering that zT value directly reflects the energy conversion efficiency, a lot of studies have focused on reducing the thermal conductivity of skutterudite in order to zT maximization for increase their efficiency [10].

Skutterudites are commonly prepared and shaped using methods like solid-state reaction [11], spark plasma sintering [12, 13], high pressure and high-temperature (HPHT) [14–17], high-temperature electrochemical synthesis [18] co-precipitation [19], sol–gel [20] and solvothermal methods [21–28]. However, the application of electrospinning technique to the preparation of unfilled or filled skutterudites is less explored.

Electrospinning is able to continuously produce nanofibers with diameters ranging from 50 to 500 nm, having the advantages of an easy implementation and versatility in the manufacture of polymeric materials, composites, and ceramics [29–31]. Electrospinning is fast developing to two directions for extending its capability of creating novel nanofibers. One is the developments of coaxial [32], side-by-side [33], tri-axial [34], and other multiple-fluid processes [35] for producing core–shell [36], Janus [37], tri-layer core–shell [38] and other multiple-chamber nanofibers [39]. The other is the combination with other traditional techniques for more possibilities in fabricating novel functional nanomaterials [40].

✉ Ana C. Ferreira, acferreira@ctn.tecnico.ulisboa.pt; Joaquim B. Branco, jbranco@ctn.tecnico.ulisboa.pt; António P. Gonçalves, apg@ctn.tecnico.ulisboa.pt | [1]Centro de Ciências e Tecnologias Nucleares, Instituto Superior Técnico, Universidade de Lisboa, Campus Tecnológico e Nuclear, Estrada Nacional 10, ao km 139.7, 2695-066 Bobadela, Portugal. [2]Centro de Química Estrutural, Instituto Superior Técnico, Universidade de Lisboa, Campus Tecnológico e Nuclear, Estrada Nacional 10, ao km 139.7, 2695-066 Bobadela, Portugal.

SN Applied Sciences (2020) 2:1616 | https://doi.org/10.1007/s42452-020-03334-5

The nanoscale of the fibers can be adjusted by varying the properties of the solution and tuning of the processing parameters [29, 30]. Nanofibers, due to their reduced size, enjoy a range of attractive properties compared to known materials, such as high ratio area/volume and flexibility of structures [40]. Moreover, the preparation of nanostructured materials [41] and the elemental doping and/or voids filling of the $CoSb_3$ matrix, namely with lanthanides or alkaline earth metals [15, 42–47], currently approaches to improve the thermoelectric properties of skutterudites and to reduce their thermal conductivity, while keeping their excellent electrical properties.

The decrease of dimensionality can produce materials that have high thermoelectric figures of merit [48]. In nanostructured materials, this can be due to the differences between the mean free paths of phonons and electrons, which can lead to the scattering of phonons at the grain boundaries while keeping the large electronic conductivity [24, 49–51]. On the other hand, theoretical calculations indicated that high figures of merit can also occur because the nanodimensions can increase the change of density of states near Fermi energy level and, consequently, increase the Seebeck coefficient. It can also contribute to a local increase of effective mass of electrons and consequently reinforce the Seebeck coefficient [52]. Indeed, many investigations demonstrated that the thermoelectric properties can be improved by nanostructuring the materials, such as Bi_2Te_3/Sb_2Te_3 superlattices thin-film thermoelectric materials [53], PbSeTe-based quantum dot superlattice structures [54] incorporating nanoscale constituents within bulk materials to form nanocomposites [55, 56] and nanosized $CoSb_3$ [41].

Doping and/or voids filling the $CoSb_3$ lead to a remarkable reduction of the lattice thermal conductivity, in particular if the voids are filled with large atoms like rare earths [13, 23, 42–45, 49, 51]. The lanthanide or alkaline earth metals presented a size consistent with the host void and the difference of electronegativity $(\chi_{Sb} - \chi_{Ln}) > 0.8$. Generally, the filler forms weak bonds with Sb, and their delocalization is responsible for the decrease of thermal conductivity. [46, 57–59]. So far, the effects of partially filled skutterudites with lanthanum, cerium, and ytterbium have been reported to possess lower thermal conductivities and better electrical transport properties than $CoSb_3$ [23, 46].

The purpose of the present work was to use nanostructure engineering in the preparation of $CoSb_3$-based skutterudites through the employment of the electrospinning technique. We fabricated for the first time $CoSb_3$ and lanthanum filled $La_{0.5}Co_4Sb_{12}$ nanofibers by applying the electrospinning followed by specific heat treatments. The structure and microstructure of the materials obtained were characterized by powder X-ray diffraction (XRD) and scanning electron microscopy with energy dispersive X-ray detection (SEM/EDS). BET measurements and temperature-programmed reduction under oxygen (O_2-TPO) and hydrogen (H_2-TPR) were used to characterize this preparation route.

2 Experimental

2.1 Synthesis

Nanofibers of $CoSb_3$-based materials were obtained by a three-step methodology: (i) electrospinning of the appropriate solution containing a mixture of $Co(NO_3)_2{\cdot}6H_2O$ (Sigma, purity 99.9%) and $Sb(CH_3COO)_3$ (Aldrich, purity 99.9%), followed by (ii) calcination and (iii) reduction steps. All the reagents were used without further purification. Solutions were prepared by mixing the starting metal salts (molar ratio Co:Sb, 1:3 or 1:5) with 42 wt.% PVP40 (AlfaAsaer, average mol wt. 40,000) in a solution of absolute ethanol (Fischer-Scientific, purity > 99.9%). To filled $CoSb_3$ with lanthanum, a third solution was prepared using $La(NO_3)_3.6H_2O$ (molar ratio La:Co:Sb, 0.125:1:5). The solutions were stirred at 50 °C for 15 min to dissolve the metal salts, cooled down to room temperature and collected in a syringe with a ~ 0.9 mm interior diameter stainless steel flat tip needle. To start the electrospinning experiments, the solution was pumped continuously using a syringe pump (KW scientific) at a rate of 1 mL h^{-1}, with an electric field of 17 kV applied between the syringe tip needle and a grounded aluminum plate placed 10 cm from the needle tip and used as a collector. The electrospun materials were subsequently calcined at 600 °C for 2 h in air atmosphere and then reduced under pure hydrogen flow (2 L h^{-1}) at 500 °C for 2 h, both at 1 °C min^{-1} heating rate (Scheme 1).

2.2 Characterization

Nitrogen gas adsorption/desorption measurements (BET) were carried out using a Micrometrics ChemiSorb 2720–ChemiSoft TPx system (30% N_2 in Helium, Air Liquid 99.9995%). Powder X-ray diffraction patterns were obtained in a Bruker D8 advance diffractometer (Cu Kα-radiation) with Bragg–Brentano geometry. The operational settings for all scans were voltage = 40 kV; current = 30 mA; 20º–80º range of 2θ using a step size of 0.03º at a scan speed of 0.06º s^{-1}. The experimental data were compared with the theoretical powder patterns simulated with the help of the Powder-Cell program. Crystalline sizes were calculated using the Scherrer's equation. The surface morphology and the particle size of the samples were obtained using a FE-SEM JEOL JSM-6500F, operating at 15 keV and 80 μA. The chemical composition was

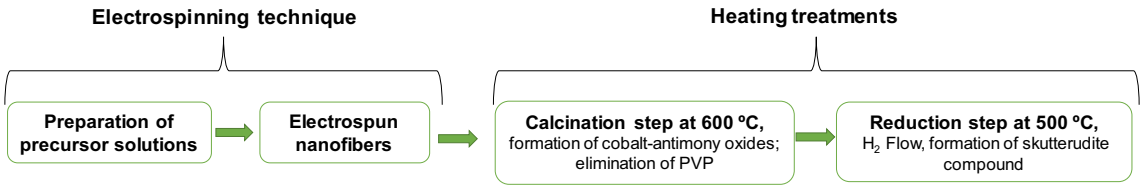

Scheme 1 Methodology steps to obtain pure skutterudite compounds

determined by a coupled EDS system. EDS composition (wt.%) was obtained from the analysis of different particles of each sample.

Thermogravimetric analysis of the electrospun material was performed on the Micromeritics ChemSorb 2720 instrument either under oxidative (O_2-TPO, temperature-programmed oxidation) or reductive (H_2-TPR, temperature-programmed reduction) conditions. Under oxidative conditions, the samples were placed in a specific Micromeritics quartz type U reactor and oxidized under a 10% O_2/helium mixture from 20 to 1000 °C, at 10 °C min^{-1} and using a total flow of 20 mL min^{-1}. The reducibility studies (H2-TPR) were also performed on the same instrument using a 10% H_2/argon mixture and the same experimental conditions. Quantitative H_2-uptakes were evaluated by integration of the experimental H_2-TPR profiles. The detector calibration response was obtained using different highly pure NiO (99.99995%, Aldrich) H_2-TPR profile areas as reference, covering our samples range of H_2 consumption.

3 Results and discussion

The analysis by SEM confirms that the collected electrospun fibers are composed of Co, Sb, C, and O, with diameters covering a range from 400 to 700 nm and slightly higher in the case of the lanthanum filled nanofibers (CoSb: 500 ± 100 nm; La-CoSb: 600 ± 100 nm) (Fig. 1a, b). After calcination, the nanofiber morphology is preserved (Fig. 1c, d) with a significant decrease of the fiber diameter (CoSb: 110 ± 20 nm; La-CoSb: 130 ± 20 nm), which is related to the decomposition of the polymer (PVP) and formation of Co-Sb (La) oxides nanofibers. After reduction, such decrease is lower (CoSb: 80 ± 10 nm; La-CoSb: 90 ± 10 nm), attributed to oxygen losses and to the formation of $CoSb_3$ and La-$CoSb_3$ nanofibers that were successfully obtained using this two-step treatment (Fig. 1e, f).

The powder XRD characterization of the collected electrospun material confirms that they have an amorphous nature (data not presented) due the high carbon content. Figure 2 shows the XRD patterns obtained for the calcined materials. These oxides present a low crystallinity but, it was possible to identify the diffraction patterns of $CoSb_2O_6$ (tetragonal phase) and α-Sb_2O_4 (orthorhombic phase), as reported on the standard JCPDS powder diffraction files [60]. It is known that the antimony acetate decomposes at 128 °C to form Sb_2O_3 and then this phase is oxidized to α-Sb_2O_4. In our case, probably all Sb_2O_3 was converted into α-Sb_2O_4 at 500 °C [61]. Other cobalt oxides phases (e.g., Co_3O_4 or CoO) were not observed.

To obtain pure $CoSb_3$, the calcined samples were treated at 600 °C under pure hydrogen atmosphere. It is important to notice that a direct treatment of the electrospun material under hydrogen implies a partial decomposition of the polymer (PVP) and end products with significant carbon impurities. Figure 3 shows the powder X-ray patterns obtained after reduction. Clearly, the use of an excess of antimony is indispensable in order to obtain pure $CoSb_3$ and the filled $CoSb_3$ with lanthanum.

Using a stoichiometric ratio of Sb/Co = 3 gives rise to the formation of the desired cubic phase of $CoSb_3$ accompanied with large quantities of impurities of the monoclinic phase of $CoSb_2$. For the ratio Sb/Co = 5, the pure body centered-cubic phase of $CoSb_3$ is the main product, with a unit cell parameter of 9.055 Å. This value is slightly higher than the values reported for the bulk material (9.034 Å) [3, 60]. In both cases, no oxides were observed but in filled skutterudite, metallic Sb was detected. Taking into account the binary Co-Sb phase diagram, on the stoichiometric ratio (75% Sb; 25% Co) the formation of pure $CoSb_3$ should occur with a stoichiometric ratio of Sb/Co = 3. However, the moderate solubility of antimony acetate in ethanol and the possibility of its volatilization referred in the literature [62–64] can explain the necessity of an excess of Sb.

The measured crystallite sizes (Scherrer's equation) were around 35 nm and from a quantitative point of view, EDS analysis confirm that the atomic ratios between metals (Sb/Co) are very close to the expected value of 3, but only when we use an excess of Sb. Tables 1 and 2 compile such XRD and EDS relevant data along with the compounds surface areas and crystallite sizes.

The formation of $CoSb_3$ and La-$CoSb_3$ nanofibers implies a two-step treatment: first, the oxidation of the electrospun material, and second, a selective treatment under hydrogen, which provides a simple, easy to implement and versatile technique to prepare novel nanostructured-based thermoelectric materials. Consequently, it was important to study

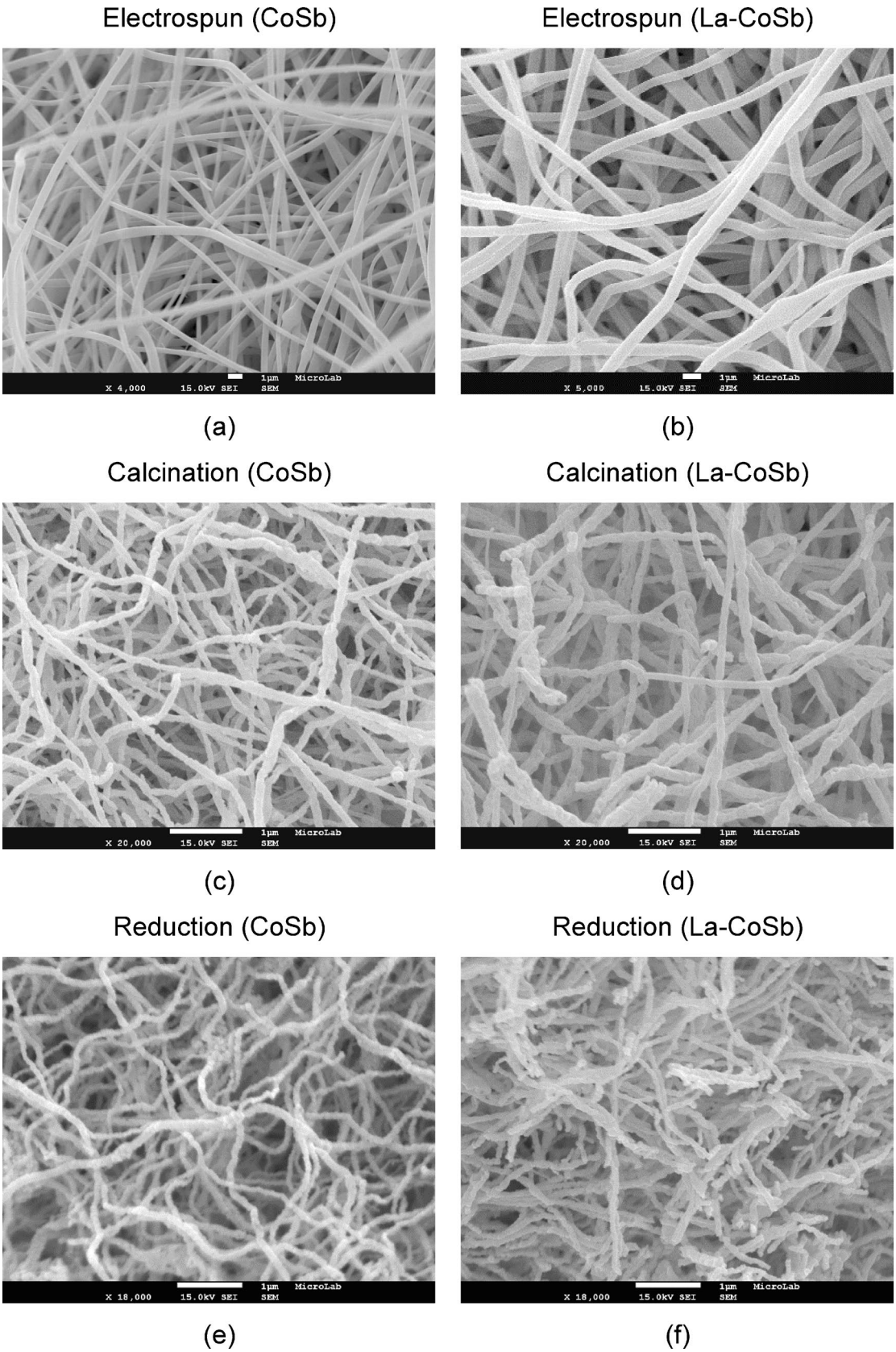

Fig. 1 SEM images of CoSb/PVP (Sb/Co = 5) and La-CoSb/PVP electrospun materials (Sb/Co = 5; La/Co = 0.125): **a**, **b** electrospun materials as collected; **c**, **d** after calcination and **e**, **f** after reduction

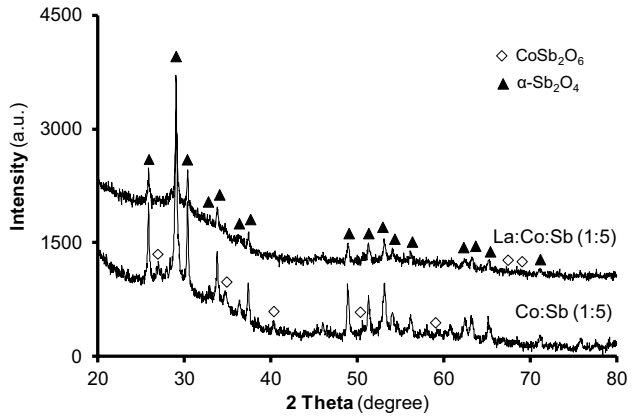

Fig. 2 XRD patterns of calcined cobalt-antimony compounds

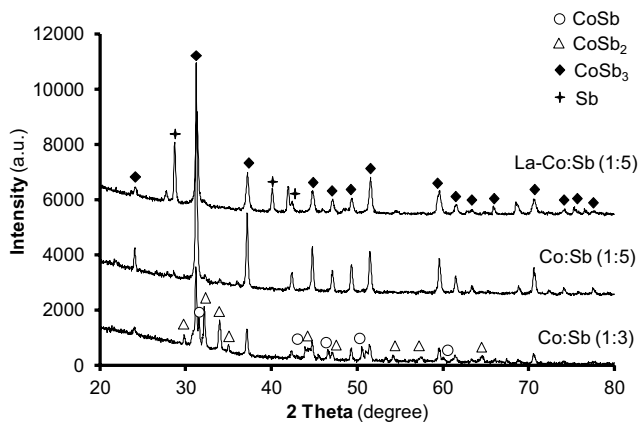

Fig. 3 XRD patterns obtained after reduction of CoSb oxides with different Sb/Co ratios and filled with lanthanum

such steps, using O_2-TPO under a 10% of O_2 in Helium, to study the formation of the CoSb and La-CoSb oxide phases, and H_2-TPR under a 10% mixture of H_2 in Argon, to study the formation of the $CoSb_3$ and La-$CoSb_3$ skutterudites.

Figure 4 shows the O_2-TPO obtained for the electrospun materials. A first stage is present in all cases the loss until 200 °C of volatile water and/or ethanol that exist in the precursor solution. A second stage (300 to 425 °C) only occurs for CoSb/PVP and La-CoSb/PVP nanofibers and correspond to the decomposition/oxidation of Co and Sb metal salts (cobalt nitrate and antimony acetate). A last stage starts at 425 °C and corresponds to the decomposition of PVP, reflecting the formation of large quantities of volatile products, e.g., CO, CO_2 and formation of the cobalt-antimony oxides. No further significant weight changes are seen above 600 °C.

Figure 5 shows the H_2-TPR profiles obtained for the selective treatment under hydrogen of the previously obtained oxides. They encompass at least three stages that we assign to the reduction of $CoSb_2O_6$ at 500–550 °C (Eq. 1), $CoSb_2O_4$ at 580–590 °C (Eq. 2) and to the reduction of antimony oxide phase (Sb_2O_4) at 590–665 °C (Eq. 3). Quantitatively, the consumption of H_2 correlates well with the theoretical values and we have found that, as expected, the ratio between experimental and theoretical H_2 uptake is close to 1 (0.91 and 0.94 for CoSb and La-CoSb oxides, respectively).

$$2CoSb_2O_6 \cdot Sb_2O_4 + 4H_2 \rightarrow 2CoSb_2O_4 \cdot Sb_2O_4 + 4H_2O \quad (1)$$

$$2CoSb_2O_4 \cdot Sb_2O_4 + 8H_2 \rightarrow 2CoSb_2 \cdot Sb_2O_4 + 8H_2O \quad (2)$$

$$2CoSb_2 \cdot Sb_2O_4 + 4H_2 \rightarrow 2CoSb_2 \cdot 2Sb + 4H_2O \quad (3)$$

$$2CoSb_2 + 2Sb \rightarrow CoSb_3 (\text{solid - state reaction}) \quad (4)$$

Table 1 Characterization of the cobalt-antimony compounds by XRD

Compounds[a]	XRD		
	Phase (main)	Lattice P. (Å)	Crystallite size (nm)
Calcined samples			
$2CoSb_2O_6.Sb_2O_4$ (1:3)	Sb_2O_4	–	–
$2CoSb_2O_6.3Sb_2O_4$ (1:5)	Sb_2O_4	a, 5.435 (5.434)[b] b, 4.808 (4.809)[b] c, 11.760 (11.779)[b]	31.8 ± 0.6[b]
$La_{0.25}.2CoSb_2O_6.3Sb_2O_4$ (1:5)	Sb_2O_4	a, 5.435 (5.434)[b] b, 4.794 (4.809)[b] c, 11.740 (11.779)[b]	30.7 ± 0.4[b]
Reduced samples			
$CoSb_3$ (1:3)	$CoSb_3$ $CoSb_2$	a, 9.057 (9.038)	33.7 ± 0.8
$CoSb_3$ (1:5)	$CoSb_3$	a, 9.055 (9.038)	36.0 ± 0.7
$La_{0.125}.CoSb_3$ (1:5)	$CoSb_3$ Sb	a, 9.029 (9.038)	24.4 ± 0.3

[a]Between parentheses the experimental Co:Sb molar ratio

[b]In the case of calcined samples the lattice parameters values and crystallite sizes corresponds to the orthorhombic phase α-Sb_2O_4. Theoretical values between parentheses

Table 2 Characterization of cobalt-antimony compounds: surface areas (BET) and EDS quantifications

Compounds[a]	BET	EDS (wt.%)[b]				
		Co	Sb	O	La	Sb/Co[c]
Calcined samples						
$2CoSb_2O_6.Sb_2O_4$ (1:3)	34.3 ± 1.3	19.4 (10.7)	65.7 (66.1)	15.0 (23.2)	–	1.6
$2CoSb_2O_6.Sb_2O_4$ (1:5)	25.1 ± 3.6	14.2 (10.7)	70.1 (66.1)	15.7 (23.2)	–	2.5
$La_{0.25}.2CoSb_2O_6.Sb_2O_4$ (1:5)	13.7 ± 0.1	12.4 (10.3)	67.7 (64.1)	10.8 (22.5)	9.1 (3.0)	2.7
Reduced samples						
$CoSb_3$ (1:3)	26.3 ± 1.4	24.6 (13.9)	75.4 (86.1)	–	–	1.5
$CoSb_3$ (1:5)	4.8 ± 0.2	14.5 (13.9)	85.5 (86.1)	–	–	2.9
$La_{0.125}CoSb_3$ (1:5)	9.1 ± 0.6	11.1 (13.3)	85.0 (82.7)	–	3.9 (3.9)	3.0

[a]Between parentheses the experimental Co:Sb molar ratio

[b]Theoretical values between parentheses, calculated take in account the compounds chemical formula

[c]Antimony/cobalt atomic ratio; theoretical value 3.0

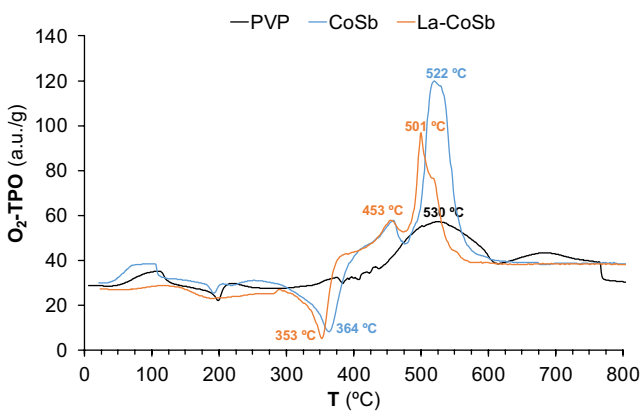

Fig. 4 O_2-TPO profiles of CoSb/PVP, La-CoSb/PVP and "pure" PVP nanofibers

Nevertheless, stability studies of such oxide phases under hydrogen and studies about their formation are rare and we have only found two that seems to confirm our reduction stage hypothesis (validated by the H_2-TPR quantitative analysis). The first reported shows that the oxidation of $CoSb_3$ leads to a formation of $CoSb_2O_4$, $CoSb_2O_6$, and Sb_2O_4 [65], whereas the second study indicates that $CoSb_2$ is the final product of the reduction of $CoSb_2O_6$ under hydrogen at temperatures ≥ 650 °C [66]. The formation of $CoSb_3$ can be explained by solid-state reaction (Eq. 4), which agrees with literature results that indicate that $CoSb_2$ acted as intermediate for the formation of $CoSb_3$ [65, 67].

Considering the improvement effect of nanostructures on thermoelectric efficiency of materials, the synthesis of unfilled and La-filled $CoSb_3$ nanofibers by electrospinning technique seem to be a good way to develop novel nanostructured skutterudite-based thermoelectric materials.

4 Conclusions

Nanosized skutterudites of the type $CoSb_3$ unfilled and La filled were successfully synthesized via electrospinning technique. A "three-step" model is suggested for the formation of the $CoSb_3$ phase, where a precursor solution was

Fig. 5 H_2-TPR profiles of $CoSb_3$ formation (1:5)

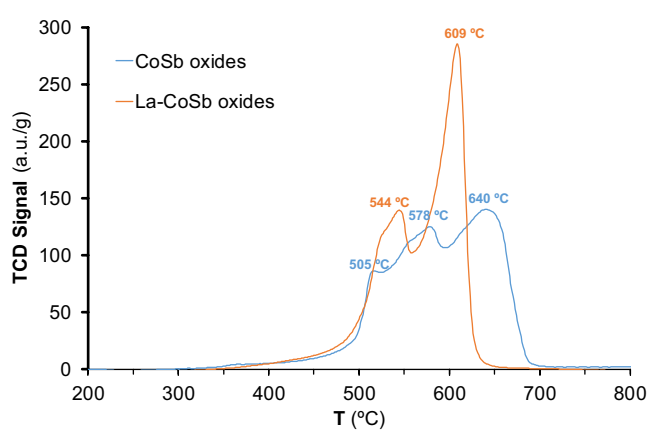

electrospun, the collected fibers were calcined at 600 °C and finally reduced at 500 °C to form $CoSb_3$ unfilled and filled with lanthanum. This preparation methodology requires the use of an excess of antimony (Sb/Co = 5). SEM observations show that the synthesized $CoSb_3$ nanofibers consist of particles with sizes of around 35 nm and their synthesis by electrospinning provides a simple and low-cost way to develop novel nanostructured skutterudite-based thermoelectric materials.

Acknowledgements Authors gratefully acknowledge the support of the Portuguese "Fundação para a Ciência e a Tecnologia", FCT, through the UID/Multi/04349/2013, PTDC/EMS-ENE/3009/2014 and PTDC/EAM-PEC/28374/2017 projects.

Funding This study was funded by Portuguese "Fundação para a Ciência e a Tecnologia", FCT, through the UID/Multi/04349/2013, PTDC/EMS-ENE/3009/2014 and PTDC/EAM-PEC/28374/2017 projects.

Compliance with ethical standards

Conflict of interest The authors declare that they have no known competing financial interests or personal relationships that could have appeared to influence the work reported in this paper.

References

1. Sharp JW, Jones EC, Williams RK, Martin PM, Sales BC (1995) Thermoelectric properties of $Cosb_3$ and related alloys. J Appl Phys 78:1013–1018
2. Uher C, Li CP, Ballikaya S (2010) Charge-compensated n-type skutterudites. J Electron Mater 39:2122–2126
3. Caillat T, Borshchevsky A, Fleurial JP (1996) Properties of single crystalline semiconducting $CoSb_3$. J Appl Phys 80:4442–4449
4. Sofo JO, Mahan GD (1998) Electronic structure of $CoSb_3$: a narrow-band-gap semiconductor. Phys Rev B 58:15620–15623
5. Anno H, Matsubara K, Notohara Y, Sakakibara T, Tashiro H (1999) Effects of doping on the transport properties of $CoSb_3$. J Appl Phys 86:3780–3786
6. Singh DJ, Pickett WE (1994) Skutterudite antimonides: quasilinear bands and unusual transport. Phys Rev B 50:11235–11238
7. Chapon L, Ravot D, Tedenac JC (1999) Nickel-substituted skutterudites: synthesis, structural and electrical properties. J Alloy Compd 282:58–63
8. Morelli DT, Caillat T, Fleurial JP, Borshchevsky A, Vandersande J, Chen B, Uher C (1995) Low-temperature transport-properties of P-type $Cosb_3$. Phys Rev B 51:9622–9628
9. Sales BC, Mandrus D, Chakoumakos BC, Keppens V, Thompson JR (1997) Filled skutterudite antimonides: electron crystals and phonon glasses. Phys Rev B 56:15081–15089
10. Yang L, Hng HH, Cheng H, Sun T, Ma J (2008) Synthesis of $CoSb_3$ by a modified polyol process. Mater Lett 62:2483–2485
11. Leithe-Jasper A, Kaczorowski D, Rogl P, Bogner J, Reissner M, Steiner W, Wiesinger G, Godart C (1999) Synthesis, crystal-structure determination and physical properties of $YbFe_4Sb_{12}$. Solid State Commun 109:395–400
12. Li XY, Chen LD, Fan JF, Zhang WB, Kawahara T, Hirai T (2005) Thermoelectric properties of Te-doped $CoSb_3$ by spark plasma sintering. J Appl Phys 98:083702
13. Yang L, Wu JS, Zhang LT (2004) Synthesis of filled skutterudite compound $La0.75Fe_3CoSb_{12}$ by spark plasma sintering and effect of porosity on thermoelectric properties. J Alloy Compd 364:83–88
14. Kihou K, Shirotani I, Shimaya Y, Sekine C, Yagi T (2004) High-pressure synthesis, electrical and magnetic properties of new filled skutterudites LnOs(4)P(12) (Ln = Eu, Gd, Tb, Dy, Ho, Y). Mater Res Bull 39:317–325
15. Puyet M, Lenoir B, Dauscher A, Dehmas M, Stiewe C, Muller E (2004) High temperature transport properties of partially filled $Ca_xCo_4Sb_{12}$ skutterudites. J Appl Phys 95:4852–4855
16. Sun HR, Jia XP, Deng L, Wang C, Lv P, Guo X, Sun B, Zhang YW, Liu BW, Ma HA (2014) Beneficial effect of high pressure and double-atom-doped skutterudite compounds $Co_4Sb11.5$-xTe0.5Sn_x by HPHT. J Alloy Compd 612:16–19
17. Sun HR, Jia XP, Deng L, Lv P, Guo X, Sun B, Zhang YW, Liu BW, Ma HA (2014) Impacts of both high pressure and Te–Se double-substituted skutterudite on the thermoelectric properties prepared by HTHP. J Alloy Compd 615:1056–1059
18. DeMattei RC, Watcharapasorn A, Feigelson RS (2001) Conditions for the electrochemical synthesis of the CoPn(3) (Pn = P, As, Sb) skutterudites. J Electrochem Soc 148:D109–D111
19. Toprak MS, Stiewe C, Platzek D, Williams S, Bertini L, Muller EC, Gatti C, Zhang Y, Rowe M, Muhammed M (2004) The impact of nanostructuring on the thermal conductivity of thermoelectric $CoSb_3$. Adv Funct Mater 14:1189–1196
20. Chu Y, Tang XF, Zhao WY, Zhang QJ (2008) Synthesis and growth of rodlike and spherical nanostructures $CoSb_3$ via ethanol sol–gel method. Cryst Growth Des 8:208–210
21. Yu SH, Yang J, Wu YS, Han ZH, Lu J, Xie Y, Qian YT (1998) A new low temperature one-step route to metal chalcogenide semiconductors: PbE, Bi_2E_3 (E = S, Se, Te). J Mater Chem 8:1949–1951
22. Deng Y, Zhou XS, Wei GD, Liu J, Nan CW, Zhao SJ (2002) Solvothermal preparation and characterization of nanocrystalline Bi_2Te_3 powder with different morphology. J Phys Chem Solids 63:2119–2121
23. Mi JL, Zhao XB, Zhu TJ, Tu JP (2008) Nanosized La filled CoSb(3) prepared by a solvothermal-annealing method. Mater Lett 62:2363–2365
24. Mi JL, Zhao XB, Zhu TJ, Tu JP, Cao GS (2006) Solvothermal synthesis and electrical transport properties of skutterudite $CoSb_3$. J Alloy Compd 417:269–272
25. Kadel K, Li WZ (2014) Solvothermal synthesis and structural characterization of unfilled and Yb-filled cobalt antimony skutterudite. Cryst Res Technol 49:135–141
26. Li Y, Li CG, Wang BB, Li WJ, Che P (2019) A comparative study on the thermoelectric properties of $CoSb_3$ prepared by hydrothermal and solvothermal route. J Alloy Compd 772:770–774
27. Bhaskar A, Yang YW, Yang ZR, Lin FH, Liu CJ (2015) Fast fabrication and enhancement of thermoelectric power factor of p-type nanostructured $CoSb_3$(1 + delta) (delta = 0.00, 0.01 and 0.02) using solvothermal synthesis and evacuating-and-encapsulating sintering. Ceram Int 41:7989–7995
28. Kumari L, Li WZ, Huang JY, Provencio PP (2010) Solvothermal synthesis, structure and optical property of nanosized $CoSb_3$ skutterudite. Nanoscale Res Lett 5:1698–1705
29. Xue JJ, Xie JW, Liu WY, Xia YN (2017) Electrospun nanofibers: new concepts, materials, and applications. Acc Chem Res 50:1976–1987
30. Xue JJ, Wu T, Dai YQ, Xia YN (2019) Electrospinning and electrospun nanofibers: methods, materials, and applications. Chem Rev 119:5298–5415
31. Aruchamy K, Mahto A, Nataraj SK (2018) Electrospun nanofibers, nanocomposites and characterization of art: insight on establishing fibers as product. Nano-Struct Nano-Objects 16:45–58

32. Wang ML, Hai T, Feng ZB, Yu DG, Yang YY, Bligh SWA (2019) The relationships between the working fluids, process characteristics and products from the modified coaxial electrospinning of zein. Polymers (Basel) 11(8):1287
33. Yu DG, Wang ML, Li XY, Liu XK, Zhu LM, Bligh SWA (2020) Multifluid electrospinning for the generation of complex nanostructures. Wires Nanomed Nanobiotecnol 12:e1601
34. Zhao K, Wang W, Yang YY, Wang K, Yu DG (2019) From Taylor cone to solid nanofiber in tri-axial electrospinning: size relationships. Results Phys 15:102770
35. Wang ML, Wang K, Yang YY, Liu YN, Yu DG (2020) Electrospun environment remediation nanofibers using unspinnable liquids as the sheath fluids: a review. Polymers (Basel) 12(1):103
36. Dogan YK, Demirural A, Baykara T (2019) Single-needle electrospinning of PVA hollow nanofibers for core-shell structures. SN Appl Sci 1:415
37. Yang JK, Wang K, Yu DG, Yang YY, Bligh SWA, Williams GR (2020) Electrospun Janus nanofibers loaded with a drug and inorganic nanoparticles as an effective antibacterial wound dressing. Mater Sci Eng C-Mater 111:110805
38. Yang YY, Chang SY, Bai YF, Du YT, Yu DG (2020) Electrospun triaxial nanofibers with middle blank cellulose acetate layers for accurate dual-stage drug release. Carbohydr Polym 243:116477
39. Chang S, Wang M, Zhang F, Liu Y, Liu X, Yu DG, Shen H (2020) Sheath-separate-core nanocomposites fabricated using a trifluid electrospinning. Mater Des 192:108782
40. Islam S, Ang BC, Andriyana A, Afifi AM (2019) A review on fabrication of nanofibers via electrospinning and their applications. SN Appl Sci 1:1248
41. Mi JL, Zhu TJ, Zhao XB, Ma J (2007) Nanostructuring and thermoelectric properties of bulk skutterudite compound $CoSb_3$. J Appl Phys 101:054314
42. Morelli DT, Meisner GP, Chen BX, Hu SQ, Uher C (1997) Cerium filling and doping of cobalt triantimonide. Phys Rev B 56:7376–7383
43. Chen BX, Xu JH, Uher C, Morelli DT, Meisner GP, Fleurial JP, Caillat T, Borshchevsky A (1997) Low-temperature transport properties of the filled skutterudites $CeFe_{4-x}Co_xSb_{12}$. Phys Rev B 55:1476–1480
44. Nolas GS, Kaeser M, Littleton RT, Tritt TM (2000) High figure of merit in partially filled ytterbium skutterudite materials. Appl Phys Lett 77:1855–1857
45. Kuznetsov VL, Kuznetsova LA, Rowe DM (2003) Effect of partial void filling on the transport properties of $NdxCo_4Sb_{12}$ skutterudites. J Phys-Condens Mater 15:5035–5048
46. Sales BC, Mandrus D, Williams RK (1996) Filled skutterudite antimonides: a new class of thermoelectric materials. Science 272:1325–1328
47. Bertini L, Stiewe C, Toprak M, Williams S, Platzek D, Mrotzek A, Zhang Y, Gatti C, Muller E, Muhammed M, Rowe M (2003) Nanostructured $Co_{1-x}Ni_xSb_3$ skutterudites: synthesis, thermoelectric properties, and theoretical modeling. J Appl Phys 93:438–447
48. Sales BC (2002) Thermoelectric materials: smaller is cooler. Science 295:1248–1249
49. Zhai PC, Zhao WY, Li Y, Liu LS, Tang XF, Zhang QJ, Niino M (2006) Nanostructures and enhanced thermoelectric properties in Ce-filled skutterudite bulk materials. Appl Phys Lett 89:052111
50. Zhao LD, Zhang BP, Liu WS, Li JF (2009) Effect of mixed grain sizes on thermoelectric performance of Bi_2Te_3 compound. J Appl Phys 105:023704
51. Alboni PN, Ji X, He J, Gothard N, Tritt TM (2008) Thermoelectric properties of La(0.9)CoFe(3)Sb(12)-CoSb(3) skutterudite nanocomposites. J Appl Phys 103:113707
52. Heremans JP, Jovovic V, Toberer ES, Saramat A, Kurosaki K, Charoenphakdee A, Yamanaka S, Snyder GJ (2008) Enhancement of thermoelectric efficiency in PbTe by distortion of the electronic density of states. Science 321:554–557
53. Venkatasubramanian R, Siivola E, Colpitts T, O'Quinn B (2001) Thin-film thermoelectric devices with high room-temperature figures of merit. Nature 413:597–602
54. Harman TC, Taylor PJ, Walsh MP, LaForge BE (2002) Quantum dot superlattice thermoelectric materials and devices. Science 297:2229–2232
55. Zhao XB, Ji XH, Zhang YH, Zhu TJ, Tu JP, Zhang XB (2005) Bismuth telluride nanotubes and the effects on the thermoelectric properties of nanotube-containing nanocomposites. Appl Phys Lett 86:062111
56. Hsu KF, Loo S, Guo F, Chen W, Dyck JS, Uher C, Hogan T, Polychroniadis EK, Kanatzidis MG (2004) Cubic AgPbmSbTe2 + m: bulk thermoelectric materials with high figure of merit. Science 303:818–821
57. Jacobsen MK, Liu W, Li B (2014) Enhancement of thermoelectric performance with pressure in $Ce_{0.8}Fe_3CoSb_{12.1}$. J Phys Chem Solids 75:1017–1023
58. Nolas GS, Slack GA, Morelli DT, Tritt TM, Ehrlich AC (1996) The effect of rare-earth filling on the lattice thermal conductivity of skutterudites. J Appl Phys 79:4002–4008
59. Sales BC (2003) Filled Skutterudites. In: Gschneidner KA Jr, Gschneidner JKA, Bünzli J-CG, Pecharsky VK (eds) Handbook on the physics and chemistry of rare earths. Elsevier Science, Amsterdam
60. JCPDS (1981) The powder diffraction file, JCPDS, 1601 Park Avenue, Swarthmore, PA
61. Liu SM, Wen B, Jiang WW, Liu CQ, Ding WY, Wang N, Chai WP (2014) Influence of calcination temperature on the structure, morphology and composition of micro alpha-Sb_2O_4 crystals. Ceram Int 40:15991–15995
62. Li H, Tang XF, Zhang QJ, Uher C (2008) Rapid preparation method of bulk nanostructured $Yb_{0.3}Co_4Sb_{12+y}$ compounds and their improved thermoelectric performance. Appl Phys Lett 93:252109
63. Yu J, Zhao WY, Wei P, Tang DG, Zhang QJ (2012) Effects of excess Sb on thermoelectric properties of barium and indium double-filled iron-based p-type skutterudite materials. J Electron Mater 41:1414–1420
64. Liu WS, Zhang BP, Li JF, Zhao LD (2007) Effects of Sb compensation on microstructure, thermoelectric properties and point defect of $CoSb_3$ compound. J Phys D Appl Phys 40:6784–6790
65. Leszczynski J, Wojciechowski KT, Malecki AL (2011) Studies on thermal decomposition and oxidation of $CoSb_3$. J Therm Anal Calorim 105:211–222
66. Jovic M, Dasic M, Holl K, Ilic D, Mentus S (2009) Gel-combustion synthesis of $CoSb_2O_6$ and its reduction to powdery Sb_2Co alloy. J Serb Chem Soc 74:53–60
67. Broz P, Zelenka F, Kohoutek Z, Vrestal J, Vykoukal V, Bursik J, Zemanova A, Rogl G, Rogl P (2019) Study of thermal stability of $CoSb_3$ skutterudite by Knudsen effusion mass spectrometry. Calphad 65:1–7